Spin-dependent tunneling conductance of Fe|MgO|Fe sandwiches

W. H. Butler, X.-G. Zhang, and T. C. Schulthess
Oak Ridge National Laboratory, Oak Ridge, Tennessee 37831-6114

J. M. MacLaren
Department of Physics, Tulane University, New Orleans, Louisiana 70018
(Received 21 June 2000; published 8 January 2001)

We present first-principles based calculations of the tunneling conductance and magnetoconductance of epitaxial Fe(100)|MgO(100)|Fe(100) sandwiches. Our results indicate that tunneling is much more interesting and complicated than the simple barrier model used previously. We obtain the following general results: (1) Tunneling conductance depends strongly on the symmetry of the Bloch states in the electrodes and of the evanescent states in the barrier layer. (2) Bloch states of different symmetry decay at different rates within the barrier. The decay rate is determined by the complex energy bands of the same symmetry in the barrier. (3) There may be quantum interference between the decaying states in the barrier. This leads to an oscillatory dependence of the tunneling current on $k_{\|}$ and a damped oscillatory dependence on barrier thickness. (4) Interfacial resonance states can allow particular Bloch states to tunnel efficiently through the barrier. For Fe(100)|MgO(100)|Fe(100) our calculations indicate that quite different tunneling mechanisms dominate the conductance in the two spin channels. In the majority channel the conductance is primarily via Bloch electrons with small transverse momentum. One particular state with Δ_1 symmetry is able to effectively couple from the Fe into the MgO. In the minority channel the conductance is primarily through interface resonance states especially for thinner layers. We predict a large magnetoresistance that increases with barrier thickness.

DOI: 10.1103/PhysRevB.63.054416 PACS number(s): 75.70.Cn, 72.15.Gd, 73.40.Gk, 73.40.−c

I. INTRODUCTION

There is presently great scientific and commercial interest in spin-dependent tunneling between ferromagnetic electrodes separated by insulating oxide barriers.[1–4] Most of the interest for applications currently centers on systems with amorphous aluminum oxide tunneling barriers because of the relative ease of growing adherent aluminum oxide without pinholes. Unfortunately these systems are difficult to characterize and model because of the noncrystalline nature of the oxide and the lack of any known epitaxial relationship between the oxide and the ferromagnetic electrodes.

Recently Heinrich *et al.* have grown Fe(100)|MgO(100)|Fe(100) magnetic tunnel junctions by depositing MgO epitaxially onto Fe whiskers and then depositing another Fe electrode epitaxially on top of the MgO.[5] They were able to demonstrate tunneling through MgO barriers that were only 5 atomic layers in thickness. Furthermore their results indicated that the transport through at least the top electrode was primarily ballistic even at room temperature. Unfortunately they were not able to measure the magnetoresistance of this system in their initial experiments.

In this paper we use first-principles electronic structure techniques to calculate the tunneling between Fe(100) electrodes separated by MgO tunneling barriers. In order to calculate the electronic and magnetic properties of Fe|MgO|Fe sandwiches it is necessary to have a reliable physical model for the interface between Fe (100) and MgO. The structure that we used is described in Sec. II. This model for the physical structure was then used for calculations of the electronic and magnetic structures. These are described in Sec. III. Based on the physical electronic and magnetic structures the tunneling conductance and magnetoconductance were calculated. The results of these calculations are described in Sec. IV.

Most previous theories of tunneling conductance and magnetoconductance have emphasized the density of states of the electrodes. The tunneling matrix elements are almost always neglected or treated as inert factors. One of our conclusions is that this approach is completely inadequate for understanding tunneling. The nature of the states both in the electrodes and in the barrier layer are extremely important in determining the tunneling conductance. Specifically we shall show that the symmetry of both the propagating states in the electrodes and of the evanescent states in the barrier material are crucial to determining the tunneling conductance. We shall also show that there may be multiple states with complex wave vectors in the insulating barrier and that these may lead to strong interference effects in the tunneling conductance. Interfacial resonance states can also strongly influence the tunneling conductance.

Because of the different character of the states at the Fermi energy in the majority and minority channels, the dominant tunneling mechanisms are quite different. In the majority channel the conductance is primarily via Bloch electrons with small transverse momentum. One particular state with Δ_1 symmetry is able to effectively couple from the Fe into the MgO and also out of the MgO into the Fe electrode on the other side. In the minority channel the conductance is primarily through interface resonance states especially for thinner layers. As the barrier becomes thicker the majority channel conductance for parallel moment alignment dominates the conductance because of the slow decay of the Δ_1 state in the MgO. This leads to a large magnetoresistance that increases with barrier thickness.

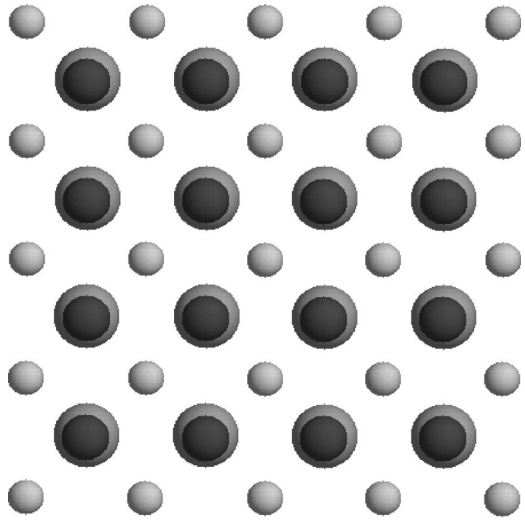

FIG. 1. Interface for Fe(100)|MgO. Larger atoms are iron. Darker atoms above iron atoms represent oxygen. Small light atoms represent magnesium.

II. STRUCTURE OF IRON–MAGNESIUM OXIDE INTERFACE

There have been several studies of the growth of MgO on Fe(100)[6–9] and of the interface between the iron and MgO. It was found both for iron deposited on MgO(100) and for MgO deposited onto Fe(100) that Fe[100] is parallel to MgO[110]. Low energy electron diffraction (LEED) studies[8] strongly suggest that the Fe atoms sit atop the O atoms when Fe is deposited onto a clean MgO (100) surface. A diagram of the interfacial structure is shown in Fig. 1. Although it was difficult to precisely determine the Fe–O separation in the LEED study a separation of 2.0 Å was considered most probable.

In addition to the experimental studies of the Fe|MgO interface we know of one theoretical study[10] which treated a monolayer and a bilayer of Fe adsorbed on an MgO surface. In that study the MgO was modeled as five (100) layers of MgO with either one or two layers of Fe placed on both sides of the MgO slab. Total energy calculations using the local spin density approximation (LSDA) to density functional theory (DFT) implemented within the full-potential linearized augmented plane wave (FLAPW) technique determined that the Fe atoms preferred to sit atop the O atoms. The predicted O–Fe distance was 2.3 Å for the monolayer and this was assumed not to change for the bilayer. Reconstruction or rumpling of the MgO layers was apparently not considered. The general picture emerging from this study was that there are only weak interactions between the electronic structures of Fe and MgO.

Our interest is centered on a slightly different structure, that of only a few MgO atomic layers deposited onto an iron substrate followed by deposition of a relatively thick Fe top electrode. Experimentally, seven atomic layers of MgO can be grown pseudomorphically[5] on Fe (100). For thicker MgO layers misfit dislocations form to partially relieve the 3.5% compressive in-plane strain that arises due to the larger MgO lattice constant. Thus the previous studies were for an interface in which the Fe lattice was expanded in-plane whereas it seems more appropriate to model this system as having interfaces in which the Fe is at its equilibrium lattice constant and the MgO layers are contracted in-plane.

We therefore performed a series of full potential LSDA–DFT calculations using the plane wave pseudopotential technique.[11] In these calculations the sandwich structure was modeled by a 15 atom/supercell with five (100) Fe layers alternating with five (100) MgO layers. The in-plane lattice constant was held equal to that calculated for LSDA–DFT bcc Fe. All atomic coordinates were allowed to relax in the direction perpendicular to the layers. These calculations yielded an Fe–O distance of 2.169 Å intermediate between that predicted by the FLAPW study and that deduced by fits to LEED data. The spacing of the first two Fe layers was found to be about 2% smaller than between the second and third Fe layers. We found only a slight (0.05 Å) displacement of the Mg atoms in the first MgO layer towards the Fe interface.

III. ELECTRONIC AND MAGNETIC STRUCTURE

In order to determine the electronic structure within a framework that could be used to determine the transmission and reflection amplitudes of Bloch waves in Fe incident on the MgO layer we used the layer Korringa–Kohn–Rostoker technique[12] which does not require the assumption of an artificial periodicity in the direction perpendicular to the layers. Four (100) layers of MgO were embedded within an Fe (100) lattice. The experimental Fe lattice constant 2.866 Å, was used for the iron lattice. The Fe–O distance was taken to be 2.16 Å. The MgO lattice constant both in-plane and out-of-plane was taken to be a factor of $\sqrt{2}$ larger than that of the Fe. The atomic potentials were represented within the atomic sphere approximation using sphere radii of 1.022 Å and 1.427 Å for Mg and O, respectively. In addition, to correctly account for the volume of each layer an empty sphere of radius 0.9476 Å was inserted in the interfacial Fe layer just below the Mg atom displaced 0.067 Å towards the Mg.

The calculation proceeded by calculating the electronic structure and Green function for bulk Fe. Then the Green function was used to embed four MgO monolayers and eight additional atomic layers of Fe (four on each side of the MgO) in the bulk Fe. The Fermi energy was maintained equal to that of the bulk iron as the self-consistent electronic structure was calculated for the entire system consisting of bulk iron plus the 12 embedded layers.

The self-consistent calculation allowed for a rearrangement of charge between the layers. This rearrangement of charge is necessary to correctly offset the bands of the MgO relative to those of Fe and is shown in Fig. 2. Here we have counted the approximately 0.5 electrons in the empty sphere near the interface as residing on the last Fe layer. We find in general agreement with the FLAPW calculations, that there is relatively little charge transfer between the Fe and the MgO. The total moment calculated for the iron atoms of the interfacial layer was approximately $3\mu_B$ which agrees with the FLAPW calculations cited previously.[10]

The electronic density of states (DOS) was calculated for

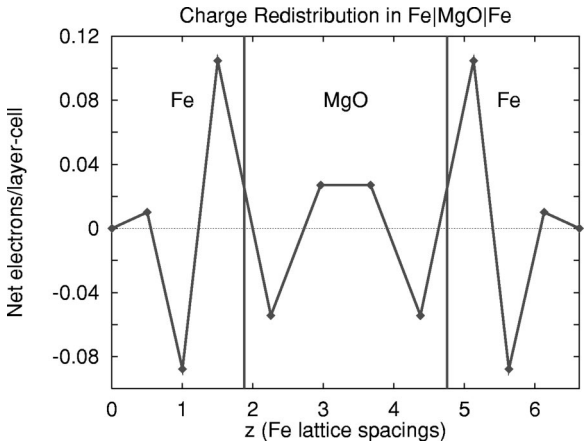

FIG. 2. Charge rearrangement in the Fe|MgO|Fe sandwich. The redistribution of charge near the interface is necessary to correctly position (in energy) the MgO potentials relative to those of the Fe.

each layer and for the majority and minority spin channels. We found that the density of states near the interface was quite different from that of the bulk and that this difference was opposite for the two spin channels as is shown in Figs. 3 and 4.

Near the interface the majority DOS is strongly reduced in the vicinity of the Fermi energy whereas for the minority

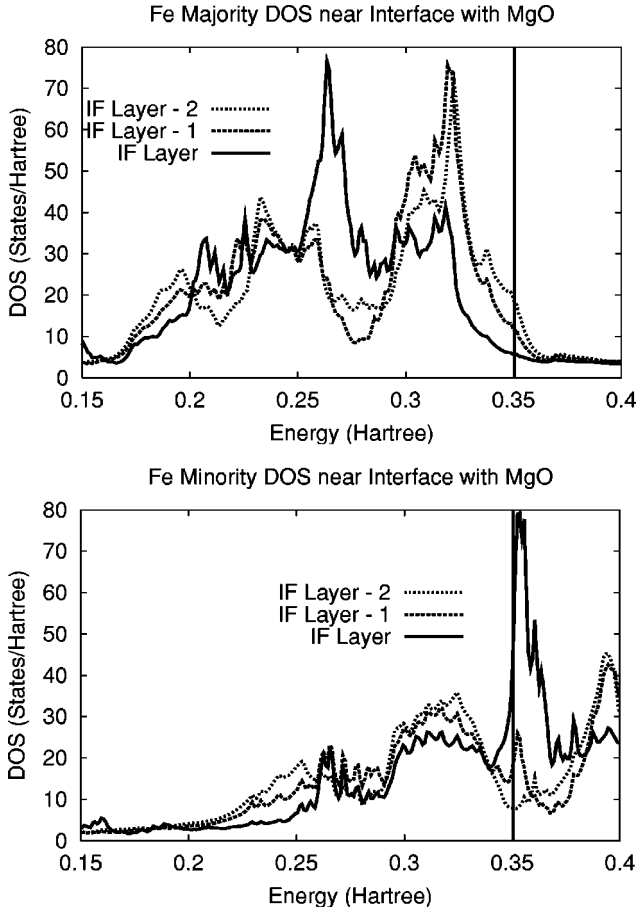

FIG. 3. Density of states for each atomic layer of Fe(100) near an interface with MgO. One hartree equals 27.2 eV.

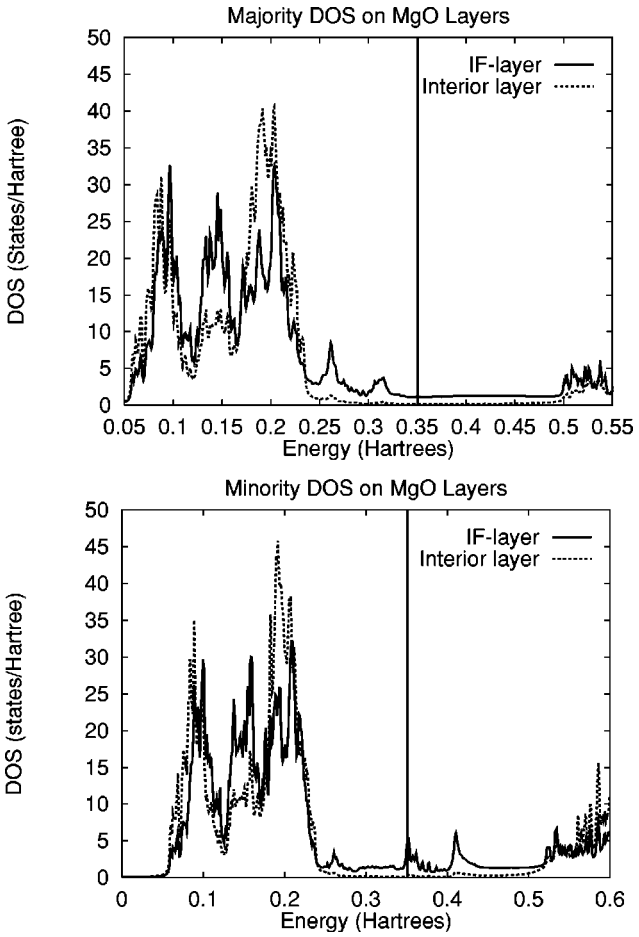

FIG. 4. Density of states for each of the atomic layers of MgO near an interface with Fe(100).

spin channel the Fermi energy falls near a sharp peak in the DOS. The FLAPW calculations previously cited[10] also show a very sharp peak in the minority DOS for the case of a single Fe layer on MgO. The general result shown here that the majority Fermi energy DOS is reduced near the interface and the minority DOS has a large peak just above the Fermi energy seems to be a common feature associated with the interface between Fe(100) and an insulator or semiconductor. We have observed qualitatively similar effects in calculations of the electronic structure of interfaces of Fe(100)|Ge,[13] Fe(100)|GaAs,[13] Fe(100)|ZnSe,[14] and Fe(100)|vacuum.[15]

The density of states for the MgO layers in the vicinity of the Fermi energy (Fig. 4) shows a wide gap in the density of states especially on the interior MgO layers that appears to be approximately 5.5 eV in width extending from 0.244 hartree to 0.446 hartree in Fig. 4. We verified the gap position and width by taking the potentials from the layer interior to the barrier region and repeating them periodically to form a bulk system. The position and width of the gap calculated this way were identical to those obtained from the DOS of Fig. 4. Similar calculations for semiconductors such as GaAs (Ref. 13) and ZnSe (Ref. 15) did not show such a well-defined gap for very thin barrier layers. The calculated gap width agrees with previous DFT–LDA calculations[16] but is

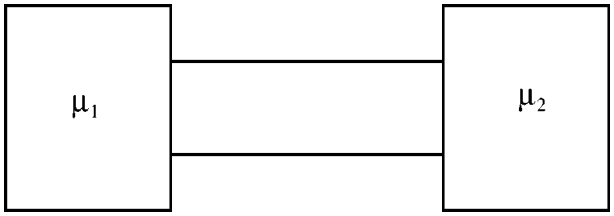

FIG. 5. Two electron reservoirs connected by a sample.

somewhat less than the experimental value of 7.8 eV.[17]

There seems to be a faint ''echo'' of the peak in the Fe minority DOS just above the Fermi energy that is visible in the minority DOS of the interfacial MgO layer. There are similar faint echos of peaks in the majority Fe DOS that can be seen in the interfacial MgO DOS near 0.26 and 0.31 hartree.

IV. TUNNELING CONDUCTANCE

We calculated the tunneling conductance by use of a very simple but general result due to Landauer[18,19] which relates the conductance to the probability of a Bloch electron in one of the Fe electrodes being transmitted through the MgO barrier layer to the opposite electrode.

To understand the Landauer conductance formula it is helpful to consider two reservoirs for electrons connected by a sample as shown in Fig. 5. The sample, in our case, would consist of the MgO tunneling barrier surrounded by the two Fe electrodes. If we imagine the left reservoir with chemical potential μ_1, to be an emitter of right going electrons, we can write the current density of those electrons that leave the reservoir on the left and enter the reservoir on the right as

$$J^+ = \frac{e}{(2\pi)^3}\int d^3k v_z^+(\mathbf{k}) f_0^+(\mu_1) T^+(\mathbf{k}), \tag{1}$$

where

$$T^+(\mathbf{k}) \equiv \sum_{k'} T^{++}(\mathbf{k}\mathbf{k}'), \tag{2}$$

and z is the direction from reservoir 1 to reservoir 2. Performing the integral over k_z yields

$$J^+ = \frac{e}{A}\sum_{k_\parallel,j}\frac{1}{2\pi}\int dk_z \frac{1}{\hbar}\frac{\partial \varepsilon}{\partial k_z} f_0(\mu_1) T^+(\mathbf{k}) \tag{3}$$

which yields an expression for the current

$$I^+ = \frac{e}{h}\int^{\mu_1} d\varepsilon \sum_{k_\parallel,j} T^+(k_\parallel, j). \tag{4}$$

Here the sum over j is needed because there will, in general, be more than one Bloch state for a given value of $k_\parallel$. A line of reasoning similar to the one that led to Eq. (4) leads to an expression for the current of electrons emitted in the $-z$ direction by the reservoir on the right which enter the reservoir on the left

$$I^- = \frac{e}{h}\int^{\mu_2} d\varepsilon \sum_{k_\parallel,j} T^-(k_\parallel, j). \tag{5}$$

Assuming time reversal invariance, we can equate T^+ and T^-. (To apply the time reversal argument rigorously we should reverse the moment directions as well as the electron directions. If we ignore spin–orbit coupling however, $T^+ = T^-$ for the individual spin channels.)This allows us to write the net current as

$$I = I^+ - I^- = \frac{e^2}{h}\sum_{k_\parallel,j} T^+(k_\parallel, j)\frac{\mu_1 - \mu_2}{e} \tag{6}$$

which yields the Landauer conductance formula

$$G = \frac{e^2}{h}\sum_{k_\parallel,j} T^+(k_\parallel, j). \tag{7}$$

The original Landauer formula has the ratio of transmission probability divided by reflection probability (T/R) where we have only the transmission probability in Eq. (7). It is now usually accepted that this additional factor of $1/R$ is present or not depending on exactly how the measurement is performed that is, on whether or not one measures current and voltage using the same leads as is assumed in the derivation here or whether a separate set of probes is used to determine the voltage across the sample. When applied to tunneling, the difference between the two formulas will usually be negligible because tunneling transmission probabilities are usually very small and the reflection probabilities are near unity.

We have already described[14] how the primitive transmission and reflection amplitudes that the layer-KKR technique uses to propagate plane waves between layers can be used to calculate the transmission and reflection amplitudes for Bloch waves. Briefly, the equations which describe plane waves reflecting from and being transmitted through the barrier are transformed into a set of equations that describe the transmission and reflection of Bloch waves. This set of equations contains both traveling and evanescent solutions of the Schrödinger equation for the crystal. Within the subspace of the traveling Bloch states however, we obtain a unitary scattering matrix. Because the scattering matrix is unitary, current is conserved and the same conductance is obtained irrespective of which two layers on opposite sides of the barrier are used to calculate the transmission probability. We consider this to be an important test of the validity of a theory of tunneling and its implementation.

A. Majority transmission probability

The calculated transmission probability as a function of $k_\parallel$ for the majority spin channel is shown in Fig. 6 for 4, 8, and 12 layers of MgO. We shall discuss the transport in this channel first because the dependence of the transmission

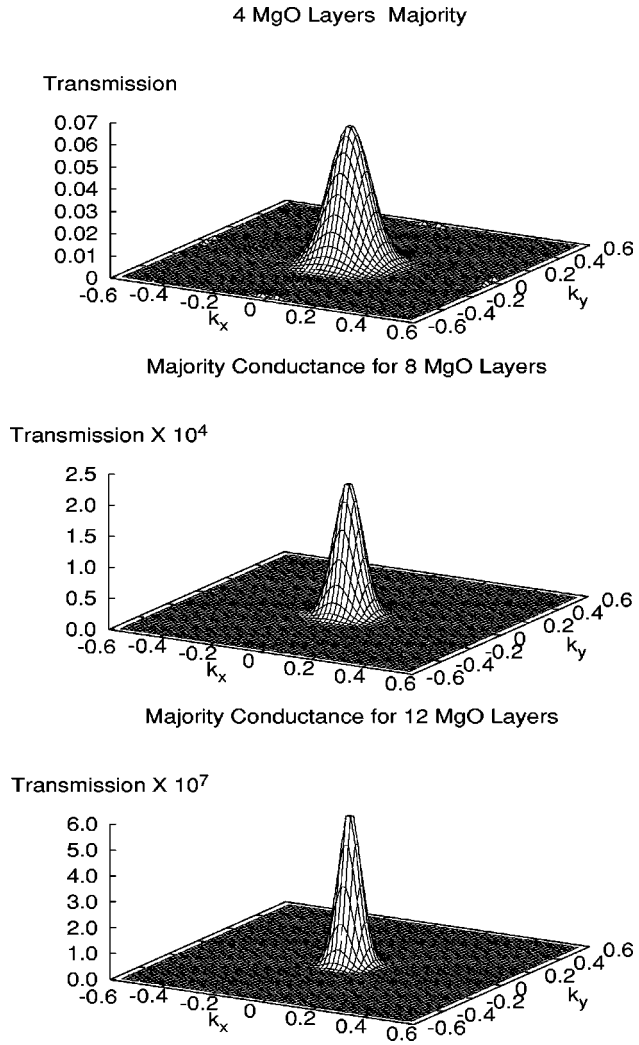

FIG. 6. Majority conductance for 4, 8, and 12 layers of MgO. Units for k_x and k_y are inverse bohr radii.

probability on $k_\parallel$ is easier to understand for the majority channel than for the minority channel or for antiparallel moment alignment.

Because of the two-dimensional periodicity, the crystal momentum parallel to the layers is conserved. For the majority channel the conductance has a rather broad peak centered at $k_\parallel=0$. A somewhat similar peak is predicted for the tunneling of free electrons through a simple square barrier.[20] The conductance observed here however differs significantly as is shown in Fig. 9 which shows the transmission probability as a function of k_x for $k_y=0$. The oscillations in transmission as a function of $k_\parallel$ will be discussed later.

One important feature that is clear from comparing the three panels of Fig. 6 is the increasing concentration of the transmission in the region near $k_\parallel=0$ as the insulating barrier layer is made thicker. This general feature would be expected from the simple model of a free electron incident on a square barrier of height V_b and thickness d for which the transmission probability contains a factor $\exp(-2d\kappa)$ where $\kappa^2=(2m/\hbar^2)(V_b-E_F)+k_\parallel^2$. In real systems the variation of the transmission is much more complicated as we shall discuss below. However the strong concentration of majority transmission near $k_\parallel=0$ and the fact that this region of the two-dimensional zone dominates the transmission for simple model barriers indicates that it is important to understand the tunneling in detail for $k_\parallel=0$.

B. Effect of symmetry at $k_\parallel=0$

In order to better understand the conductance we examine the *tunneling* DOS for $k_\parallel=0$ for the individual energy bands. We define the tunneling density of states (TDOS) to be the density of electronic states subject to the following boundary conditions: on the left-hand side of the interface there is an incoming Bloch state with unit flux and the corresponding reflected Bloch states; on the right-hand side are the corresponding transmitted Bloch states. Figure 7 shows the TDOS associated with each of the Fe(100) Bloch states having $k_\parallel=0$.

The tunneling density of states plots illustrate several novel features of tunneling in real systems. Consider first the issue of symmetry. Both the majority and minority channels have four Fe(100) Bloch states for $k_\parallel=0$. In the majority channel there is a Δ_1 state, a doubly degenerate Δ_5 state, and a $\Delta_{2'}$ state. The minority channel has four states with the same symmetries as the states of the majority channel with the crucial exception that the majority Δ_1 state is replaced by a Δ_2 minority state. This information of course is available by simple inspection of a band structure calculation for bulk Fe.

The decay rates for each of the Fe(100) Bloch states within the MgO can be determined by inspection of a band structure plot as is illustrated in Fig. 8. In this figure, $k^2(E)$ along the [100] (Δ) direction is plotted for energies in the vicinity of the gap for bulk MgO. In this case, k^2 was calculated using the LKKR code with the potentials for bulk MgO taken from a center layer of the Fe(100)|MgO(100)|Fe(100) sandwich in order to correctly place the Fermi energy within the gap but any calculation for the band structure of bulk MgO would suffice for obtaining a qualitative understanding of the decay rates. Figure 8 shows $(k\Delta z)^2$ where Δz is the interplanar spacing for MgO(001) and k is in the (001) direction. The figure shows $(k\Delta z)^2$ for the three symmetries (Δ_1, Δ_5, and $\Delta_{2'}$). For each symmetry we plot only the complex band with the smallest values of $|k^2|$ in the vicinity of the Fermi energy. The nearest complex band with symmetry Δ_2 would cross the Fermi energy with a value of $-(k\Delta z)^2$ of approximately 31.5. The energy range for which all values of k^2 are less than zero is the energy gap. The remaining symmetry in the (001) direction, $\Delta_{1'}$, which is not represented in Fe or MgO near the Fermi energy has a minimum angular momentum of $l=4$ and presumably only yields a real band at very high energy. It would correspond to a state that decays extremely rapidly.

It can be seen that the slowest decay rate is for states with Δ_1 symmetry which are predicted to decay at the rate $\exp(-2\kappa\Delta z)$ where $\kappa\Delta z=\sqrt{-(k_{\Delta_1}\Delta z)^2}\approx 1.47$. Band states in MgO with Δ_1 symmetry occur at both the bottom and the top of the energy gap. Δ_1 states transform like linear combinations of functions with $1, z$, and $2z^2-x^2-y^2$ symmetry.

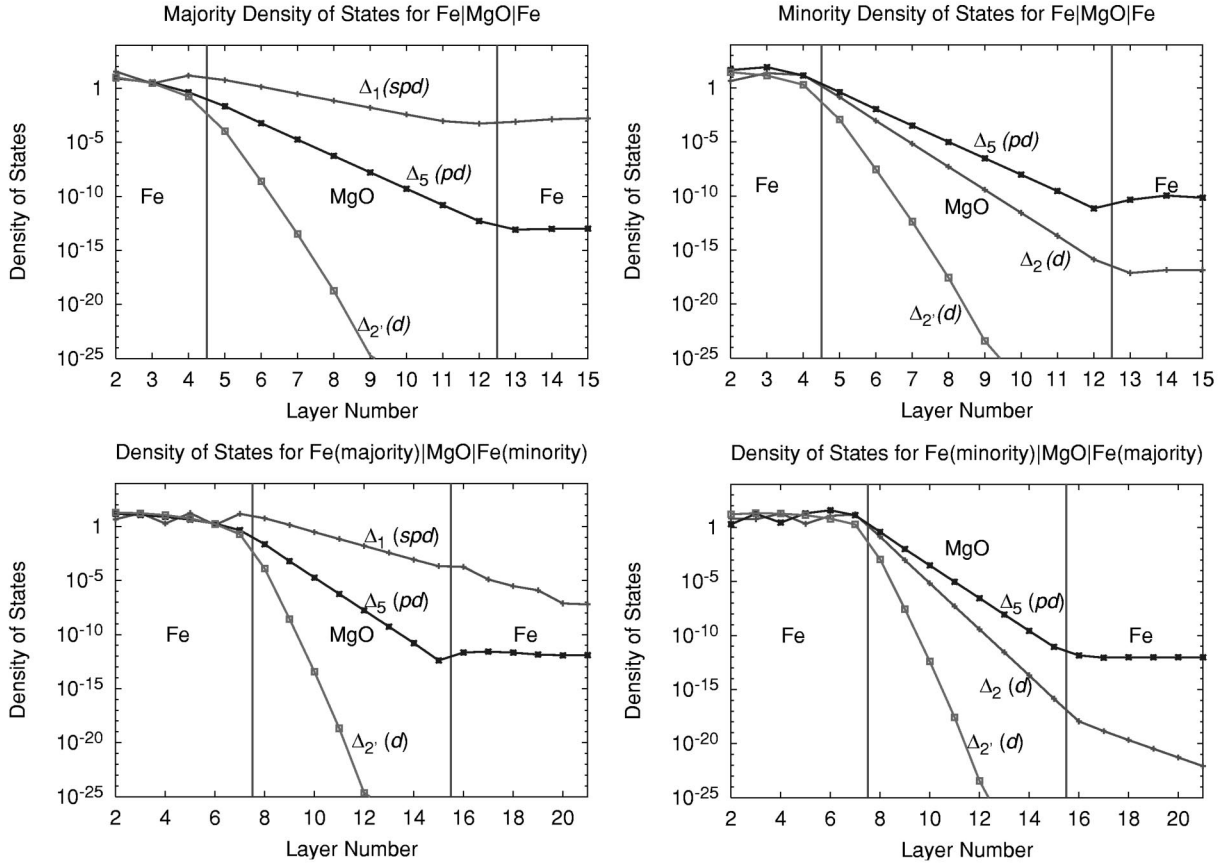

FIG. 7. Tunneling DOS for $k_{\|}=0$ for Fe(100)|8MgO|Fe(100). The four panels show the tunneling DOS for majority (upper left) minority (upper right), and antiparallel alignment of the moments in the two electrodes (lower panels). Additional Fe layers are included in the lower panels to show the TDOS variation in the Fe. Each TDOS curve is labeled by the symmetry of the incident Bloch state in the left Fe electrode.

The next slowest decay rate is for states with Δ_5 symmetry. There is a high mass Δ_5 band at the top of the valence band. These states are doubly degenerate and transform like linear combinations of functions with zx and zy symmetry. The $\Delta_{2'}$ state becomes a band state about 2.7 eV above the bottom of the conduction band. However, it becomes real at the X point ($k\Delta z=\pi$); thus π has been subtracted from $k\Delta z$ for the $\Delta_{2'}$ state for the purposes of plotting the decay rates in Fig. 8.

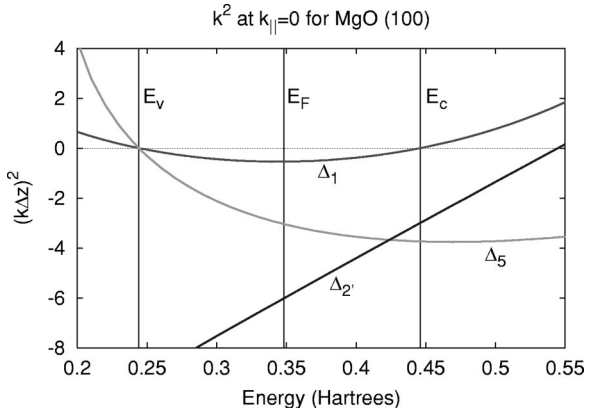

FIG. 8. Dispersion $k^2(E)$ for MgO in the vicinity of the gap along Δ (100). Negative values of k^2 determine the exponential decay rates for various Bloch states. E_v is top of valence band. E_c is the bottom of the conduction band.

Majority Bloch states with Δ_1 symmetry in the Fe electrodes decay as evanescent states with Δ_1 symmetry in MgO. Similarly Δ_5 Bloch states which occur for both majority and minority Fe(100) decay as evanescent states with the same symmetry in the MgO. The $\Delta_{2'}$ Bloch states which have xy symmetry and which occur in both the majority and minority Fe(100) channels however, decay as Δ_2 states in the MgO. Similarly, the $\Delta_{2'}$ states (y^2-z^2 symmetry) decay as Δ_2 states in the MgO. The reason for this is not a mysterious change in the symmetry of the wave functions but is due to the fact that the MgO cubic cell is rotated by $\pi/4$ with respect to that of the Fe, thus states with $x'y'$ symmetry in Fe have x^2-y^2 symmetry in MgO where (x,y) and (x',y') are related by a $\pi/4$ rotation.

The results of these symmetries can be seen in Fig. 7. Consider first the upper panels which show the tunneling DOS for the two spin channels for parallel alignment of the moments in the two electrodes. Only the majority channel has the slowly decaying Δ_1 state. Thus its conductance is much higher than that of the minority channel. The next slowest decay is that of the Δ_5 states which are present in

both channels. Both majority and minority Fe channels have a $\Delta_{2'}$ state that couples to a Δ_2 state in the MgO where it decays very rapidly because there are no (real) Δ_2 bands near the Fermi energy. Finally there is a minority Fe Δ_2 state that couples to a $\Delta_{2'}$ state in the MgO and then decays faster than the Δ_5 state but not so fast as the Δ_2 state. The decay rates for all of the states are given precisely by the complex energy bands of Fig. 8.

In the vicinity of the gap k^2 can be represented by

$$\frac{1}{k^2(E)} = \frac{\hbar^2}{2m_v^*(E-E_v)} + \frac{\hbar^2}{2m_c^*(E_c-E)}, \tag{8}$$

where E_v and E_c are the top of the valence band and the bottom of the conduction band, respectively, for the Δ_1 band. m_c and m_v are the effective masses for these states at the band edges. For the Δ_5 band E_v is the top of the valence band and E_c is the energy of a Γ_{15} state about 15 eV above the top of the conduction band. For the Δ_1 band Eq. (8) is in almost exact agreement with the calculated complex energy band if we use $m^*/m=0.3782$ for both the conduction and the valence band. The Δ_5 band is only given approximately by Eq. (8); however it can be rendered accurately by including second order terms in $E-E_v$ and E_c-E in the denominators. Thus it should be possible to estimate the decay rates for spin-dependent tunneling from the band structure of the barrier material. (An alternative to plotting $k^2(E)$ in the vicinity of the gap edges would be to fit the bands in the vicinity of the gap with a model Hamiltonian that yields an analytic expression for the bands in the vicinity of the gap and then solving the resulting secular equation for k_z as a function of E). The use of a band structure determined experimentally, for example, from photoemission,[21] should lead to accurate decay rates within insulating barriers.

C. Interference of tunneling states

It is generally believed that the simple barrier model is appropriate for describing the tunneling of electrons through insulating barriers. In the preceding section we showed contrary to that model, that states with different symmetry decay at different rates as they tunnel through the barrier. In this section we address the variation of the tunneling current with $k_\parallel$ and show that the barrier model fails for this aspect of tunneling as well. Figure 6 gives an overall representation of the majority tunneling current throughout the two-dimensional Brillouin zone. However, additional detail and structure can be seen if the transmission is presented on a logarithmic scale as is shown in Fig. 9.

According to the theory for tunneling through a simple barrier the transmission should vary with $k_\parallel$ as $\exp(-2d\kappa)$ where d is the thickness of the barrier and κ is given by[20]

$$\kappa^2 = \frac{2m^*}{\hbar^2}(E_b-E) + k_\parallel^2 = \kappa_0^2 + k_\parallel^2 . \tag{9}$$

A comparison of this result with the calculated transmission is shown in Fig. 9. It can be seen that the initial decrease is much faster than would be expected by the standard theory.

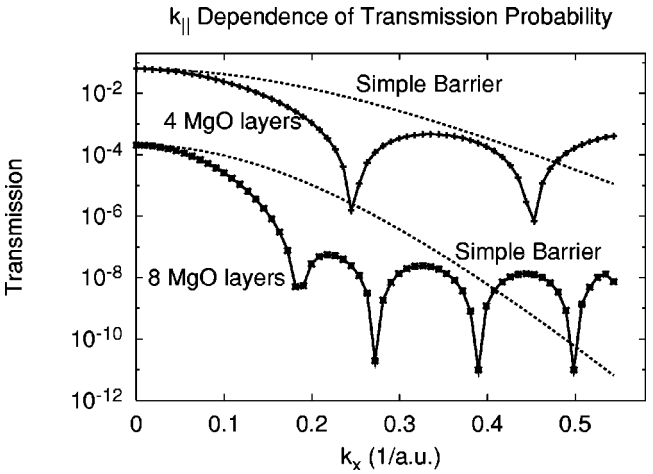

FIG. 9. Majority transmission probability as a function of $k_\parallel$ for $k_y=0$ for 4 and 8 layers of MgO. The curves end before the zone boundary is reached because there are no states for $k_x > 0.55$ (a.u.)$^{-1}$. Smooth curves show the expected behavior of the transmission probability from Eq. (9).

For larger values of k_x the calculated decrease is much slower than predicted by the standard theory. In fact it appears that the $k_\parallel$ dependence is oscillatory as if there were wave interference within the barrier.

The oscillations in the transmission that occur as a function of $k_\parallel$ result from the complex band structure of MgO in the energy gap. The complex values of k_z at the Fermi energy are plotted as a function of $k_\parallel$ in Fig. 10. The two states shown have the lowest value of the imaginary part of k_z and are therefore the most important for determining the transmission probability. The states are plotted as a function of $k_\parallel$ along $\overline{\Gamma}$ to $\overline{X}$. At $k_x=0$ the two states shown are the Δ_1 and one of the Δ_5 states. As k_x increases from zero their real part increases linearly from zero and is the same for both states.

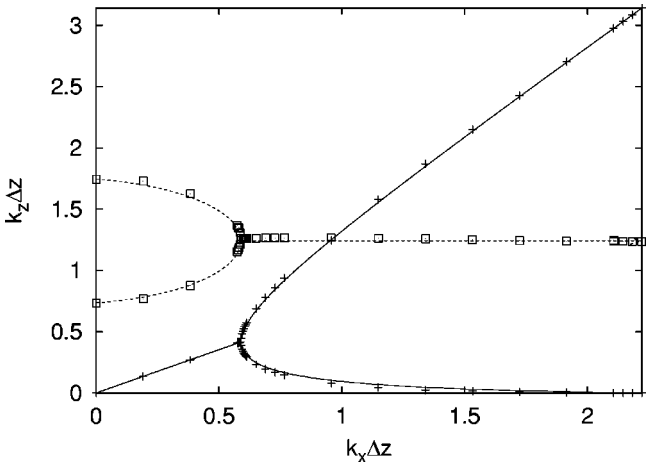

FIG. 10. Real and imaginary parts of k_z plotted as a function of k_x for MgO. The two values of k_z with the smallest imaginary parts are shown. Plus symbols (squares) denote values of the real (imaginary) part of k_z calculated with the layer KKR code. The solid line and dotted lines are the real and imaginary parts, respectively, of the fit to complex k_z described in the text.

At $k_x\Delta z \approx 0.59$ the imaginary parts become equal and the real parts bifurcate. Afterwards the imaginary part remains approximately constant. The real parts of $k_z\Delta z$ are equal to π and 0 at the zone boundary which occurs at $k_x\Delta z = \pi/\sqrt{2}$. The smooth curves which provide a good fit to the complex values of k_z are the given by the formula

$$\theta_z - i\overline{\theta_0} = \frac{\theta_x}{\sqrt{2}} \pm a\sqrt{(\theta_x - \eta)(\theta_x + \xi)}, \tag{10}$$

where $\theta_z = k_z\Delta z$ and $\theta_x = k_x\Delta z$. The constants $\overline{\theta_0}$, a, η, and ξ are determined in the following way: $\overline{\theta_0} = (\theta_z^{\Delta_1} + \theta_z^{\Delta_5})$ is the average of the two imaginary roots for $\theta_x = 0$. η is the value of θ_x for which the curves in Fig. 10 bifurcate. a and ξ are determined by the difference of the two imaginary roots at $\theta_x = 0$ and by the requirement that $\theta_z = \pi$ or 0 at $\theta_x = \pi/\sqrt{2}$.

The behavior of the complex values of k_z shown in Fig. 10 leads to the interesting interference effects shown in Fig. 9. For $k_x\Delta z$ less than 0.59 the transmission is predicted to decay as $|\psi|^2$ where $\psi = \exp(ik_1 d) + \exp(ik_2 d)$ where k_1 and k_2 represent the two complex k_x-dependent values of k_z. Thus for $k_x\Delta z < 0.59$ a.u.,

$$|\psi|^2 = e^{-2\kappa_1 d} + e^{-2\kappa_2 d} + 2e^{-\kappa_1 d - \kappa_2 d}, \tag{11}$$

where $\kappa_{1(2)} = \mathrm{Im}[k_{1(2)}(k_x)]$. Thus for $k_x\Delta z < 0.59$ a.u. the decay of the transmission follows a sum of exponentials law as a function of thickness and decreases much faster with $k_\parallel$ than would be expected from Eq. (9). On the other hand, for $k_x\Delta z > 0.59$ a.u. the imaginary parts of k_1 and k_2 are equal so that

$$|\psi|^2 = 2e^{-2\kappa(k_x)d}\{1 + \cos[k_1^r(k_x) - k_2^r(k_x)]d\}, \tag{12}$$

where k_1^r and k_2^r are the real parts of the two values of k_z. Thus the transmission is a damped oscillatory function of thickness and is a purely oscillatory function of k_x since κ is essentially independent of k_x for $k_x\Delta z > 0.59$ a.u.

We find it interesting that only a few layers of MgO seem to be sufficient that the complex energy bands of bulk MgO determine the decay of the states in the barrier and determine the dependence of the transmission on $k_\parallel$. It is also interesting that in this particular case, the transmission as a function of $k_\parallel$ switches discretely between an exponential and an oscillatory form. We have seen similar oscillatory behavior for transmission through ZnSe tunneling barriers so we suspect that this may be a general feature of tunneling through real materials.

This type of behavior can arise in the following way. If the dispersion relation in the vicinity of the gap is described within a tight binding model we expect that it can be expressed as a polynomial in $\cos(\theta_z)$ with real coefficients that depend on θ_x. The roots of this polynomial must be either real or they must occur as pairs that are complex conjugates. If the roots with the smallest imaginary part are complex conjugates r, r^* then the values of θ_z can be found from

$$z^2 - 2rz + 1 = 0, \quad z^2 - 2r^*z + 1 = 0, \tag{13}$$

where $z = e^{\theta_z}$. Each of these equations has two roots $z_1^{\pm} = r \pm \sqrt{r^2 - 1}$, $z_2^{\pm} = r^* \pm \sqrt{(r^*)^2 - 1}$. Because $z_1^+ z_1^- = z_2^+ z_2^- = 1$ we know that only two of these roots will represent decaying waves. Thus if $|z_1^+| < 1$ it follows that the two decaying roots, z_1^+ and z_2^+, have equal modulus $|z_1^+| = |z_2^+|$. Thus, the imaginary parts of θ_z for these two solutions will be equal. This would lead to the observed interference effect. Note that this does *not* explain why the imaginary part of θ_z is almost independent of θ_x.

D. Tunneling through interface resonance states

Although the $k_\parallel$ dependence of the majority channel conductance has at least superficial similarity to that of free electrons incident on a simple barrier the minority channel conductance (Fig. 11) is completely different. The complicated sharply peaked structure arises from the interplay of interfacial resonance states, the $k_\parallel$ dependence of the wave function decay in the MgO (including interference effects), and the symmetry of the minority Fe Bloch states relative to that of the complex energy bands of MgO.

We have already discussed tunneling interference along the line $k_y = 0$ in the two-dimensional Brillouin zone. We can begin to understand the effects of the interfacial resonance states by comparing the density of states on the interfacial iron layer with the transmission. These are shown as contour plots for the four MgO layer system in Fig. 12.

The interfacial density of states is quite different from that of the bulk. It is large in a ring surrounding the $\overline{\Gamma}$ point in the two-dimensional zone. The maximum values occur along the lines $k_x = 0$ and $k_y = 0$. These maxima correspond to interfacial resonance states as can be seen from Fig. 13 which is a plot of the density of states on each layer for the value of $k_\parallel$ corresponding to the peaks in Fig. 12. It can be seen that the states in the vicinity of the peak are strongly localized at the Fe–MgO interface. This is true for both the state at the peak in the interfacial DOS ($k_x = 0.299$, $k_y = 0.000$) and the state at the peak in the transmission ($k_x = 0.308$, $k_y = 0.018$). Minority Fe has only one Bloch state at the Fermi energy in this part of the two-dimensional zone.

It is clear that the interfacial resonance state is important to the transmission because it yields a huge wave function amplitude at the interface. It is equally clear however that it is only part of the story because the transmission is actually quite low for the value of $k_\parallel$ for which the DOS of the interfacial resonance is highest. The second major factor determining the transmission is the wave function symmetry. Figure 14 shows the tunneling density of states both at the peak in the interfacial density of states and at the peak in the transmission. There is a large difference in the rate of decay of the TDOS in the two cases. The tunneling DOS at the peak in the interfacial DOS ($k_x = 0.299$, $k_y = 0$) decays rapidly whereas the tunneling DOS only a slight distance away (in reciprocal space) decays very slowly. An analysis of the wave function character shows that the Bloch state at $k_x = 0.299 k_y = 0$ has no *s*-character. It can only couple to an evanescent state in the MgO that decays rapidly. Very slightly out of the $k_y = 0$ plane however, the wave function has significant *s*-character and can couple to an evanescent

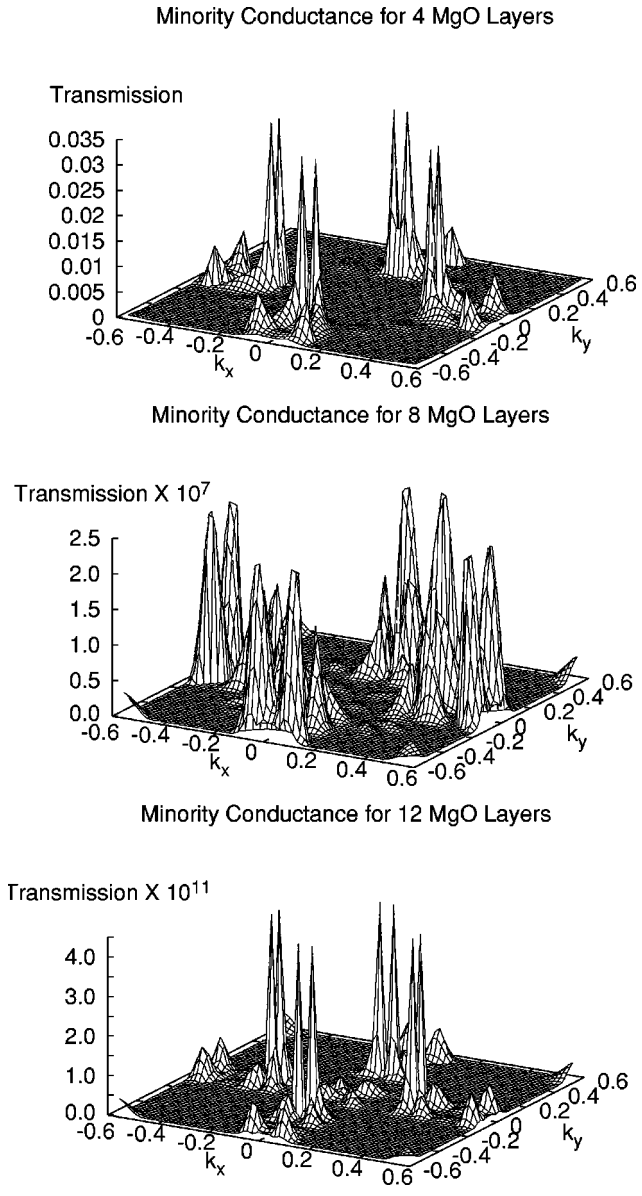

FIG. 11. Minority conductance for 4, 8, and 12 layers of MgO.

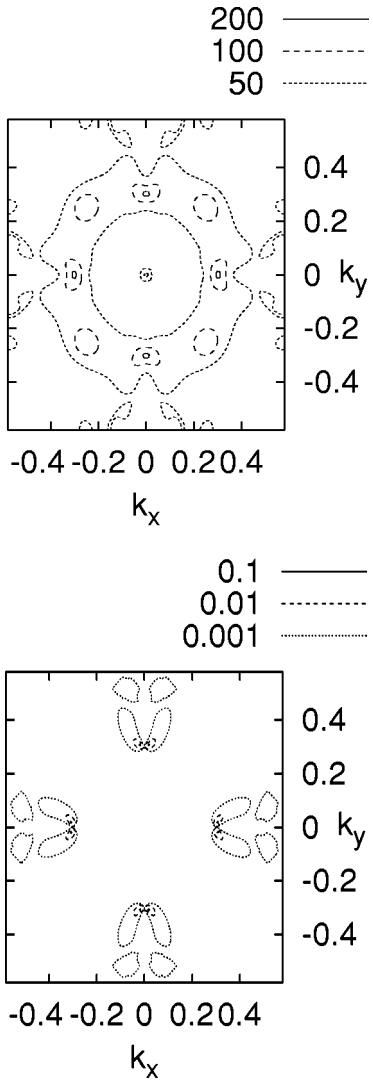

FIG. 12. Minority density of states (states/hartree) on the interfacial Fe layer (left panel) transmission in the minority channel (right panel). Units of k_x and k_y are inverse bohr radii.

state that decays slowly. The third major factor controlling the minority transmission is the tunneling interference effect discussed in Sec. IV C. Since the major interface resonances occur near the $k_y=0$ line and for $k_x>0.154$ $(k_x\Delta z>0.59)$ the analysis of that subsection shows that the $k_\parallel$ variation of the transmission should be modulated by an oscillatory function that varies with thickness.

E. Conductance for antiparallel alignment

The transmission as a function of $k_\parallel$ for antiparallel alignment of the moments (Fig. 15) shows a combination of the features observed in the majority and minority channels. For thinner layers the highest transmission is near the line $k_y=0$ in the two-dimensional zone where there is an interfacial resonance state. As the layers become thicker the highest transmission occurs closer to the origin of the two-dimensional zone due to the slow decay in the MgO of states derived from the Fe majority Δ_1 band.

Even for the thickest MgO barrier that we investigated however, the maximum conductance for antiparallel alignment did not occur exactly at $k_\parallel=0$. The reason for this can be understood from the bottom two panels of Fig. 7 which show the tunneling density of states for antiparallel alignment and $k_\parallel=0$. The total band-to-band transmission probability is the same whether calculated for electrons going left to right or right to left. This implies of course, that one must have bands of the same symmetry on both sides in order for electrons to be transmitted. Consider the majority bands on the left-hand side of the lower left panel of Fig. 7. The Δ_1 electrons readily enter the MgO where they decay slowly with distance as discussed in Sec. IV B. On the right-hand side of the barrier however these states cannot propagate because there are no minority Δ_1 propagating states at the Fermi energy. Therefore they continue to decay within the minority Fe leading to total reflection of the Δ_1 Bloch state.

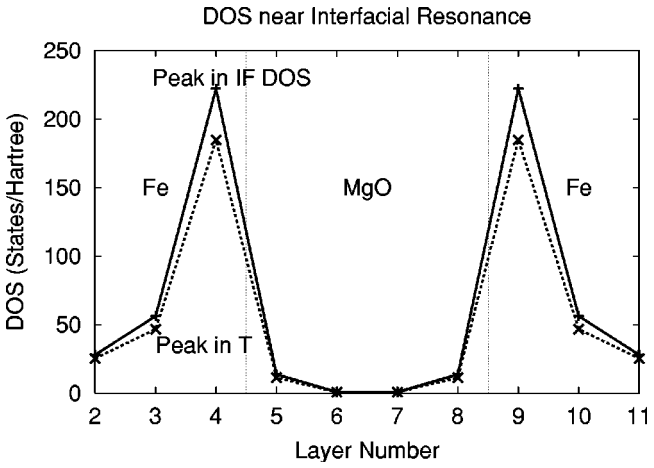

FIG. 13. Density of states on each layer for value of $k_{\|}$ equal to that of the peak in minority interfacial density of states (higher values) and for the value of $k_{\|}$ equal to the peak in the transmission (lower values)..

The Δ_5 electrons decay relatively rapidly in the MgO but they are able to enter the minority iron relatively easily because there are states to receive them. The $\Delta_{2'}$ electrons decay extremely rapidly in the MgO as discussed for the cases of majority and minority conductance.

Similarly considering now the lower right panel of Fig. 7, the minority Δ_2 state decays as a $\Delta_{2'}$ state within the MgO and continues to decay within the majority Fe layer because there is no Δ_2 state at the Fermi energy in majority Fe. Again the Δ_5 electrons decay rapidly but can enter the minority Fe while the minority Fe $\Delta_{2'}$ electrons decay extremely rapidly.

F. Thickness dependence of conductance and magnetoconductance

The conductance of the majority-parallel minority-parallel and of either channel for antiparallel alignment is shown in Fig. 16. The conductance is calculated from Eq. (7) by summing the transmission probability over the two-dimensional zone. For all thicknesses the majority conductance overwhelms the minority or the antiparallel although, for very thin barriers, the minority and antiparallel are much closer than for thicker barriers. This is due to the conductance from the interfacial resonance states which is particularly important for very thin barriers. According to our calculations the magnetoconductance should increase with thickness with the conductance becoming dominated by the majority channel.

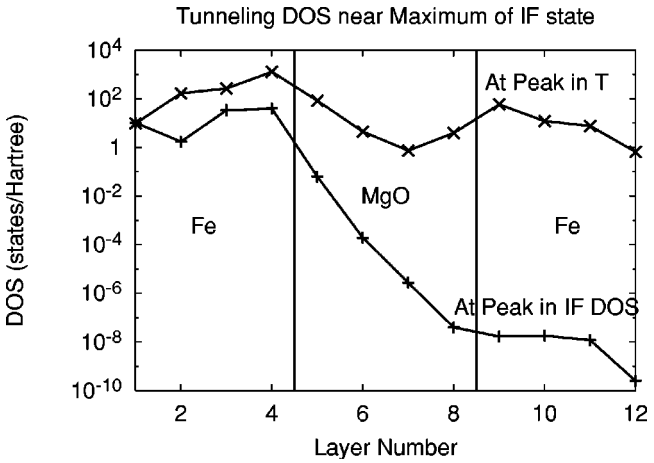

FIG. 14. Tunneling density of states at two neighboring points in the two-dimensional zone. One point is at the peak in the transmission ($k_x=0.308$, $k_y=0.018$). The other is at the peak in the interfacial density of states ($k_x=0.299$, $k_y=0.000$).

V. CONCLUSIONS

We have studied the physical electronic, magnetic, and transport properties of the Fe(100)|MgO(100)|Fe(100) system. We find a relatively small transfer of charge between the Fe and the MgO and a large modification of the density

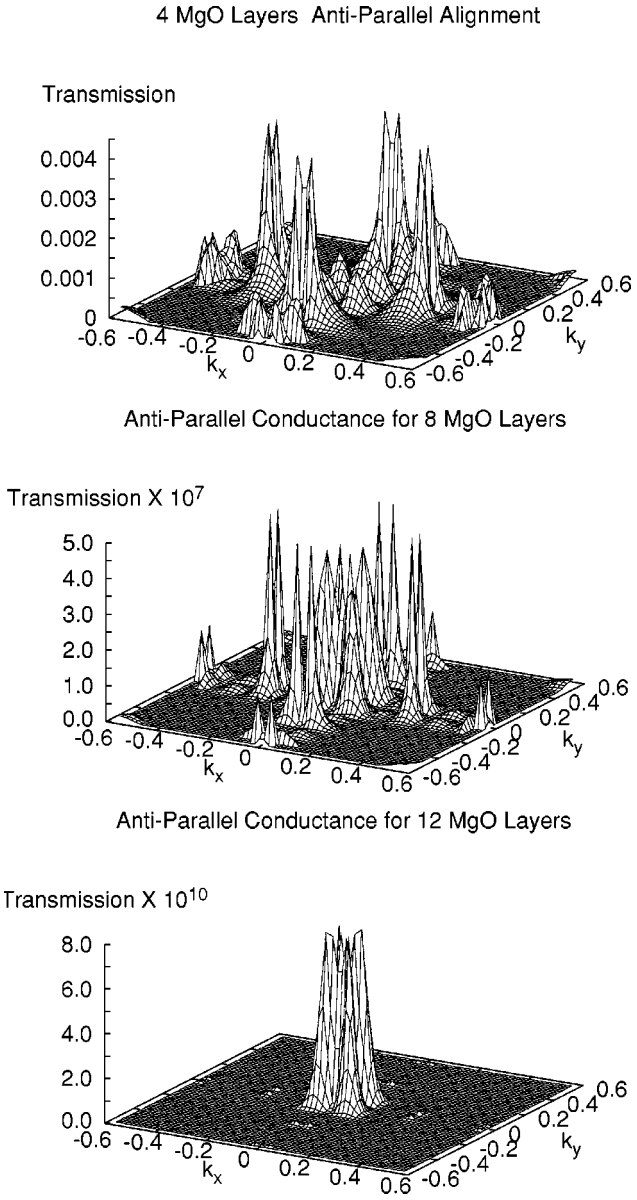

FIG. 15. Conductance for antiparallel alignment of the moments in the electrodes.

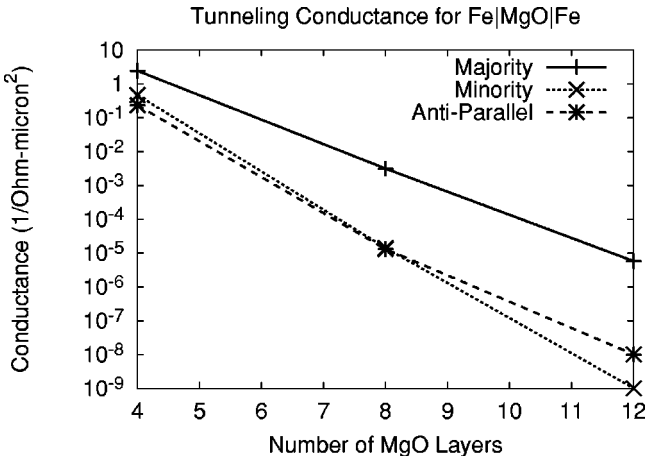

FIG. 16. Conductance as a function of the number of MgO layers.

of states near the interface. In the majority channel the Fermi energy DOS is significantly depleted on the Fe interfacial layer. In the minority channel a large peak forms on the interfacial layer just above the Fermi energy.

In calculating the tunneling conductance we encountered the following results which we believe to apply rather generally to tunneling in epitaxial systems and to be contrary to the simple barrier model that is typically used to describe electron tunneling: (1) The symmetry of the Bloch states at the Fermi energy and their relationship to the symmetry of the slowly decaying evanescent states in the barrier layer are crucial to understanding tunneling conductance. Note that for electrons with $k_{\|}=0$, these states and their symmetries can be obtained from ordinary band structure calculations. (2) There will typically be more than one evanescent state in the barrier layer at the Fermi energy. It is possible even likely, that the tunneling conductance will be affected by interference between these states. It is not yet clear to us whether this interesting prediction can be observed experimentally. (3) Interfacial resonance states can, through their effect on the wave function matching at the interface, significantly enhance the tunneling probability.

Results that are particular to tunneling through epitaxial insulators on Fe(100) include (1) majority channel tunneling is dominated by the transmission through a Δ_1 state at small values of transverse crystal momentum. (2) Minority channel tunneling is smaller and is strongly enhanced for values of $k_{\|}$ near interfacial resonance states. (3) Tunneling magnetoresistance increases with thickness. Conclusions (2) and (3) are tempered by the caveat that the interfacial resonance states seem to be very sensitive to the details of the interface.

Insights that may be relevant to the more general problem of tunneling through nonepitaxial barriers include the observation that the state with the slowest decay rate in the barrier is typically one with significant *s*- or free-electron character. Thus the reason that the tunneling conductance has been shown to be dominated by majority electrons in those cases where the spin dependence of the conductance could be determined by use of a superconducting electrode may simply be that for most of the magnetic transition metals and their alloys the majority Fermi energy DOS has more free-electron or *s*-like character than the minority which is typically predominantly *d*-like. The reason that the *d* electrons do not tunnel efficiently is that they have a much higher decay rate in the barrier because of their additional in-plane oscillations.

An additional general observation is that all other parameters being equal tunneling rates are higher if there are similar or identical states on both sides of the barrier. Thus the tunneling electrons need not only to get through the barrier but there must be a state of the correct symmetry on the other side to accept them. This may be part of the reason for the commonly observed decrease in the tunneling magnetoresistance with bias. As the bias increases the states on opposite sides of the barrier for parallel alignment differ more.

Note added in proof. We have learned that very recent XRD studies [H. L. Meyerheim (private communication)] indicate that a substochiometric layer of FeO may form at the interface between Fe(100) and MgO. At this point it is not clear if this is a general feature of this interface or to what extent its existence depends on synthesis conditions. Most of our conclusions would not be affected by this interfacial layer. The part of our calculations that we expect to be most sensitive to interfacial details are the interfacial resonance states and the tunneling conductance associated with them.

ACKNOWLEDGMENTS

Work at Oak Ridge was sponsored by the Defense Advanced Research Projects Agency and by the Office of Basic Energy Sciences Division of Materials Sciences of the U.S. Department of Energy. Oak Ridge National Laboratory is operated by UT-Battelle LLC for the U.S. Department of Energy under Contract No. DE-AC05-00OR22725. J.M.M. acknowledges support from the Oak Ridge Institute for Science and Education and DARPA Grant No. MDA 972-97-1-003. Helpful conversations with P. Dederichs concerning complex energy bands, with M. Weinert concerning surface states, and with C.-L. Fu concerning the Fe–MgO interface are gratefully acknowledged. We also thank D. M. Teter for checking the VASP calculations of the Fe–MgO interface.

[1] S. A. Rishton, Y. Lu, R. A. Altman, A. C. Marley, X. P. Bian, C. Jahnes, R. Viswanathan, G. Xiao, W. J. Gallagher, and S. S. P. Parkin, Microelectron. Eng. **35**, 249 (1997).

[2] S. S. P. Parkin, K. P. Roche, M. G. Samant, P. M. Rice, R. B. Beyers, R. E. Scheuerlein, E. J. O'Sullivan, S. L. Brown, J. Bucchigano, D. W. Abraham, Y. Lu, M. Rooks, P. L. Trouilloud, R. A. Wanner, and W. J. Gallagher, J. Appl. Phys. **85**, 5828 (1999).

[3] J. S. Moodera, E. F. Gallagher, K. Robinson, and J. Nowak, Appl. Phys. Lett. **70**, 3050 (1997).

[4] C. T. Tanaka, J. Nowak, and J. S. Moodera, J. Appl. Phys. **86**, 6239 (1999).
[5] T. L. Monchesky, A. Enders, R. Urban, J. F. Cochran, B. Heinrich, W. Wulfhekel, M. Klaua, F. Zavaliche, and J. Kirschner, in *The Physics of Low Dimensions*, edited by Jose Luis Moran Lopez (Plenum, New York, 2000); W. Wulfhekel, M. Klaua, D. Ullmann, F. Zavaliche, J. Kirschner, R. Urban, T. Monchesky, and B. Heinrich, Appl. Phys. Lett. (to be published).
[6] T. Kanaji, K. Asano, and S. Nagata, Vacuum **23**, 55 (1973).
[7] T. Kanaji, T. Kagotaini, and S. Nagata, Thin Solid Films **32**, 217 (1976).
[8] T. Urano and T. Kanaji, J. Phys. Soc. Jpn. **57**, 3043 (1988).
[9] J. F. Lawler, R. Schad, S. Jordan, and H. van Kempen, J. Magn. Magn. Mater. **165**, 224 (1977).
[10] C. Li and A. J. Freeman, Phys. Rev. B **43**, 780 (1991).
[11] These calculations were performed using the Vienna Ab-Initio Simulation Package (VASP) written by G. Kresse and J. Furthmüller; G. Kresse and J. Hafner, Phys. Rev. B **47**, 558 (1993); **49**, 14 251 (1994); G. Kresse and J. Furthmüller, Comput. Mater. Sci. **6**, 15 (1996); Phys. Rev. B **54**, 11 169 (1996).
[12] J. M. MacLaren, S. Crampin, D. D. Vvedensky, R. C. Albers, and J. B. Pendry, Comput. Phys. Commun. **60**, 365 (1990).
[13] W. H. Butler, X.-G. Zhang, X.-D. Wang, J. van Ek, and J. M. MacLaren, J. Appl. Phys. **81**, 5518 (1997).
[14] J. M. MacLaren, X.-G. Zhang, W. H. Butler, and X. Wang, Phys. Rev. B **59**, 5470 (1999).
[15] W. H. Butler, X.-G. Zhang, and J. M. MacLaren (unpublished).
[16] U. Schönberger and F. Aryasetiawan, Phys. Rev. B **52**, 8788 (1995).
[17] R. C. Whited, C. J. Flaten, and W. C. Walker, Solid State Commun. **13**, 1903 (1973).
[18] R. Landauer, IBM J. Res. Dev. **1**, 223 (1957); R. Landauer, Philos. Mag. **21**, 863 (1970).
[19] S. Data, *Electron Transport in Mesoscopic Systems* (Cambridge University Press, Cambridge, 1995).
[20] J. M. MacLaren, X.-G. Zhang, and W. H. Butler, Phys. Rev. B **56**, 11 827 (1997). The simple dependence on $\exp(-2d\kappa)$ is valid in the limit that this quantity is much less than unity.
[21] M. Grass, J. Braun, and G. Borstel, Surf. Sci. **334**, 215 (1995).